Increasing the Heat Transfer on a Grooved Surface Under Dry and Wet Conditions Using Jet Impingement

Abdulrahman S Alghamdi

Thesis submitted to the faculty of the Virginia Polytechnic Institute and State University in partial fulfillment of the requirements for the degree of

Master of Science

In

Mechanical Engineering

Thomas E. Diller, Committee Chair

Michael W. Ellis

Scott T. Huxtable

04/15/2020

Blacksburg, VA

Keywords: Array Jet Impingement Cooling, Power Plant, Air-Cooled Condensers, Jet Impingement, Discharge Coefficient, Coefficient of Performance, Grooved Surface, Cooling Towers, Hybrid Cooling, Water Consumption, Total Area, Open Area.

Increasing the Heat Transfer on a Grooved Surface Under Dry and Wet Conditions Using Jet Impingement

Abdulrahman S Alghamdi

Abstract:

An approach to hybrid cooling technique is proposed using air jets which impinge on a triangular grooved surface with dry grooves and grooves containing water. One major application is for condensers of thermoelectric power plants. The heat and mass transfer analogy was successfully used to evaluate the simultaneous heat and mass transfer. Results showed that hybrid jet impingement produced high heat flux levels at low jet velocities and flow rates. Experimental results were used to characterize the resulting heat transfer under different conditions such as flow open area percentage, array orifices diameter and array to surface stand-off distance. The results have shown that jet impingement is capable of delivering high transfer rates with lower cooling cost rates compared to current industry conventional techniques. Water is efficiently used in hybrid jet impingement because evaporative energy is absorbed directly from the surface instead of cooling air to near wet-bulb temperature.

Increasing the Heat Transfer on a Grooved Surface Under Dry and Wet Conditions Using Jet Impingement

Abdulrahman S Alghamdi

General Audience Abstract:

Array jet impingement cooling experiments were conducted on a triangular grooved surface with the surface at a constant temperature. Results showed that jet impingement can provide high transfer rates with lower rates of cooling cost in comparison to contemporary conventional techniques in the industry. Experiments on the triangular grooved surfaces were performed at dry and wet surface conditions. Under the dry conditions, the objective is to characterize the resulting heat transfer under varying operational conditions such as jet speed, array orifice diameter, array to surface stand-off distance, and flow open area percentage. Results from the triangular surface when dry showed less improvement in heat transfer than the rectangular grooved surface. A hybrid cooling technique approach was proposed and developed by using air jets impinging on a triangular grooved surface with the grooves containing water. The approach is being suggested and experimentally tested for its viability as an alternative to thermoelectric power plant cooling towers. Convection heat and mass transfer coefficients were experimentally measured for different wet coverage of the surface. Results showed that the hybrid jet impingement produced high heat flux levels at low jet velocities and flow rates. The highest heat transfer was consistently found with a 50% coverage of the surface. Hybrid jet impingement showed an improvement up to 500% in heat transfer as compared to jet impingement on a dry grooved surface

Acknowledgements

I would like to acknowledge professor Thomas E. Diller and my committee members for their advice and guidance which both were essential to completing this thesis. I also would like to acknowledge my lab mates Abdulmohsen Alsaiari and Mohammed Alanazi for their collaboration and attention. I would like to acknowledge Saudi Arabian Cultural Mission for providing the financial support that was imperative for my studies at Virginia Tech.

Table of Contents

Acknowledgements iv

Table of Contents v

List of Figures vi

List of Tables vii

Introduction: 1

Experimental setup: 3

Data Analysis: 7

Data Uncertainty: 10

Results and Discussion: 11

Conclusions: 24

Nomenclatures: 25

References 28

Appendix: 30

List of Figures

Figure 1: Abstract depiction of the experiment apparatus

Figure 2: Jets arrays all at $A_o = 1.5\%$ and different diameters.

Figure3: Jets arrays at $A_o = 1\% \ and \ 3\%$ and fixed diameters

Figure 4: Test plate

Figure 5: Top view of test Plate with guard plate and thermocouples locations

Figure 6: Energy balance and heat transfer mechanisms in hybrid jet impingement cooling

Figure 7: Plate dimensions

Figure 8: Ave h vs V for H/de = 5.4 cm, de =4.76mm, A_o= 1.5%.

Figure 9: Ave h vs V for H/de= 7.18 cm, de=4.76mm, A_o= 1.5%.

Figure 10: Ave h vs V for H/de = 5.4 cm, de =3.18mm, A_o= 1.5%.

Figure 11: Ave h vs V for H/de = 5.4 cm, de =6.35mm, A_o= 1.5%.

Figure 12: Ave h vs V for H/de = 5.4 cm, de =4.76mm, A_o= 1% and 3%.

Figure 13: q_{air} vs A_w/A_t for H/d_e= 5.4 cm, d_e=4.76mm, A_o= 1.5%.

Figure 14: Ave h vs A_w/A_t for H/d_e= 5.4 cm, d_e=4.76mm, A_o= 1.5%.

Figure 15: q_{air} vs A_w/A_t for H/d_e= 7.18 cm, d_e=4.76mm, A_o= 1.5%.

Figure 16: Ave h vs vs A_w/A_t for H/d_e= 7.18 cm, d_e=4.76mm, A_o= 1.5%.

Figure 17: q_{air} vs A_w/A_t for H/d_e= 12 cm, de=4.76mm, A_o= 1.5%.

Figure 18: Ave h vs A_w/A_t for H/d_e= 12 cm, d_e=4.76mm, A_o= 1.5%.

Figure 19: q_{air} vs A_w/A_t for H/d_e= 5.4 cm, d_e=3.18mm, A_o= 1.5%.

Figure 20: Ave h vs A_w/A_t for H/d_e= 5.4 cm, d_e=3.18mm, A_o= 1.5%.

Figure 21: q_{air} vs A_w/A_t for H/d_e= 5.4 cm, d_e=6.35mm, A_o= 1.5%.

Figure 22: Ave h vs A_w/A_t for H/de= 5.4 cm, de=6.35mm, A_o= 1.5%.

Figure 23: q_{air} vs A_w/A_t for H/d_e= 5.4 cm, d_e=4.76mm, A_o= 1%.

Figure 24: Ave h vs A_w/A_t for H/d_e= 5.4 cm, d_e=4.76mm, A_o= 1%.

Figure 25: q_{air} vs A_w/A_t for H/d_e= 5.4 cm, de=4.76mm, A_o= 3%.

Figure 26: Ave h vs A_w/A_t for H/d_e= 5.4 cm, d_e=4.76mm, A_o= 3%.

Figure 27: q_{air} vs A_o for V= 5 m/s, H/d_e= 5.4 cm, de=4.76mm.

Figure 28: q_{air} vs d_e for V= 5 m/s, H/d_e= 5.4 cm, A_o= 1.5%.

Figure 29: q_{air} vs H/d_e for V= 5 m/s, de=4.76mm, A_o= 1.5%.

List of Tables

Table 1: Measured discharge coefficients.

Table 2: Uncertainty sources for the wet surface**.**

Table 3: Reynolds number.

Table 4: CP values

Experimental Study of an Array of Jets Impinging on a Surface with Triangular Grooves on a Constant Temperature for a Hybrid Dry/Wet Cooling Approach for Thermoelectric Power Plants Condensers

Abdulrahman Alghamdi
Department of Mechanical Engineering, Virginia Tech, Heat Transfer Measurements Laboratory,

338 Goodwin Hall, 635 Prices Fork Road Blacksburg – MC 0238, VA 24061; bosha18@vt.edu

Abdulmohsen Alsaiari
Department of Mechanical Engineering, King Abdul Aziz University, Jeddah 21589, Saudi Arabia; aoalsaiari@kau.edu.sa

Thomas E. Diller*
Department of Mechanical Engineering, Virginia Tech, 313C Goodwin Hall, 635 Prices Fork Road

– MC 0238, Blacksburg, VA 24061; tdiller@vt.edu

Introduction:

Achieving a high convective heat transfer coefficient has been one of the challenges in the field of mechanical engineering. Thermal power generation faces adverse consequences because of increasing environmental temperature and cooling water supplies decreasing. The location of numerous power plants permits water use from rivers, lakes or seas for cooling. Federal regulations, however, limit new plants from using water for cooling because of the ecological concerns. This situation leads researchers to use new technologies with less water consumption or take the advantage of air as a sole coolant for cooling purposes. The condenser plays a significant role in thermal power plants. Higher power plant efficiency depends on maintaining low pressure and temperature condensation. Air-cooled condensers (ACC) rely on environmental conditions for heat rejection. When the surrounding environmental air temperature increases, the temperature difference between the atmosphere and the condenser surface decreases. The heat rejection capacity of the condenser consequently decreases, which leads to decreasing efficiency of the thermal power plant. In 2010, U.S geological experts estimated that 38% of the total fresh water consumption was used by the thermoelectric power generation [1]. In the summer of 2011 and 2012, a number of power plants in the U.S were shut down due to rising ambient air temperature [2].

Many industrial applications use the advantage of jet impingement because the boundary layer is thin in the stagnation regions. This situation creates higher heat transfer coefficients on the surface. Surface modifications are one way to improve the transfer of heat from jet impingement. Heat transfer and impingement cooling flow have been discussed in a number of studies [3]. Flat and smooth surfaces have been studied in the past [3-8] and some studies have investigated curved surfaces [9,10]. Roughened walls have been tried to enhance the heat transfer on the surface [11]. Parallel rectangular ribs were one method to create a roughened wall [11]. In some cases, enhancement in heat transfer was significant for the rectangular ribs with a single impinging jet [11]. In other cases, however, the heat transfer was reduced because the jet can be trapped in the cavity between neighboring ribs when the slot-width-to-rib-height was small. Furthermore, there is an ideal spot in between neighboring rectangular ribs to induce air bubbles in the cavity where penetration of impinging jets can be prevented into the cavity and the recirculation inside. Consequently, heat transfer can be reduced significantly [11].

A large surface area for heat transfer is provided by the Air-cooled condensers (ACC), but with a low heat transfer coefficient. Evaporative cooling towers can be used with higher ambient temperatures, but this requires a lot of make-up water [12]. An improvement of 68% in the air-to-steam flow rate decreased the thermal resistance of the air side by 66%. However, the thermal efficiency gain was negated as a result of increased pressure drop and increased fan power [13]. They also reported that jet impingement brings potential to ACC's and can provide enhancement with comparable flow rates and fan power. They suggested a hybrid condenser to conserve water, which consists of an ACC and a cooling tower to use in case of high ambient temperatures. An ACC and cooling tower can be operated as separate units, or the ACC can be operated inside the cooling tower [14]. An alternative option is to use evaporation with ACC for cooling the inlet airside with sprays [15]. A major enhancement of the thermal performance was conducted by this technique. However, there are some disadvantages if there is incomplete evaporation of the spray droplets [16]. The coefficient of performance CP was defined as the ratio of heat transfer to fan power. High coefficients of performance CP > 3000 were observed by [1] when using water-filled rectangular channels with jet impingement.

The current study represents a new approach to cooling the condensers of thermal power plants using hybrid dry/wet jet impingement. An array of air jets is proposed with water-containing triangular grooves on the air-side of a grooved plate condenser surface which is an improvement of rectangular grooves of [1]. The advantage of using the triangular ribs is to provide a wider opened spacing than rectangular ribs. Air bubbles may not be as easily formed as in the case of rectangular ribs, which would allow for higher heat transfer. The objective of the current study is to assess the feasibility of this hybrid wet/dry jet impingement system by quantifying consumption of energy and water. In a single, easy-to-operate unit, a hybrid wet/dry jet impingement condenser will provide efficient, dry and wet evaporative cooling.

Experimental setup:

Figure 1 illustrates the experimental system for measuring the average surface heat transfer from an array of impinging air jets. Air was provided by an axial flow fan through a small wind tunnel. The static pressure in the plenum was measured by a manometer and the pressure was controlled to satisfy the chosen velocities. The jet arrays were created with aluminum orifice plates. At the start of each experiment the air pressure was set by adjusting the fan speed to give the desired jet velocity. The velocity was calculated from the measured pressure difference between the plenum and the surrounding environment as:

$$V = \sqrt{\frac{2\,\Delta P}{\rho}} \qquad (1)$$

where ρ is the air density.

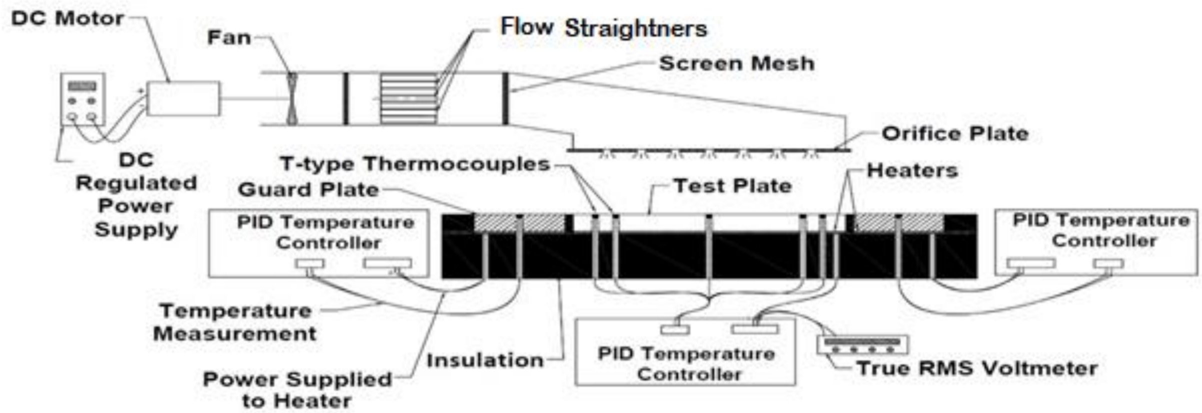

Figure 1: Abstract depiction of the experiment apparatus.

The different hole patterns used in the experiments are shown in figure 2. The ratio between the test plate surface area and the area of the orifices is defined as the open area.

$$A_o = \frac{C_d\ N\ d_e^2\ \frac{\pi}{4}}{A} \tag{2}$$

where C_d is the discharge coefficient, N is the number of jets. d_e is the effective diameter and A is the surface area of the test plate. Experiments were conducted using open areas of $1\%, 1.5\ \%$, and 3%, with orifice diameters of 3.18 mm, 4.76mm and 6.35mm. Because of the contraction of the flow as it turns through the orifice, most jet arrays are produced using orifices in thin plates with discharge coefficients of $C_D = 0.75$ to 0.85, This gives an effective diameter of:

$$d_e = \sqrt{c_D}\ d \tag{3}$$

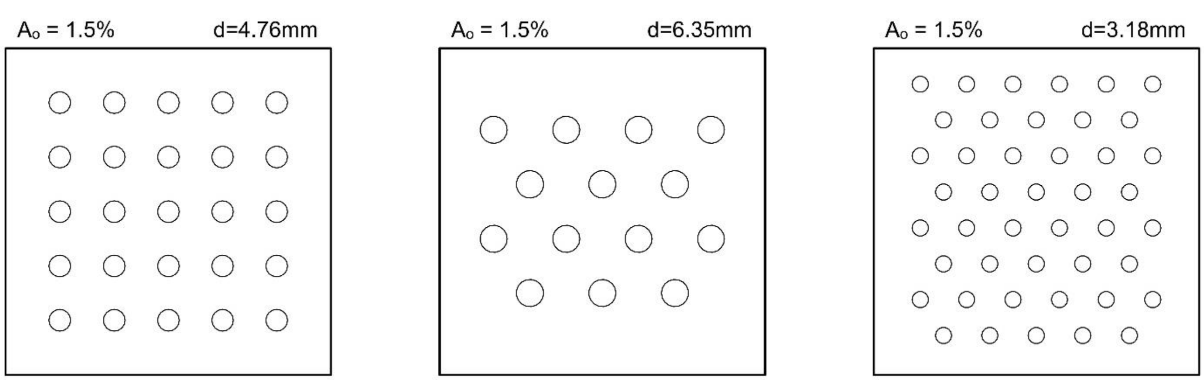

Figure 2: Jets arrays at $A_o = 1.5\%$ and different diameters.

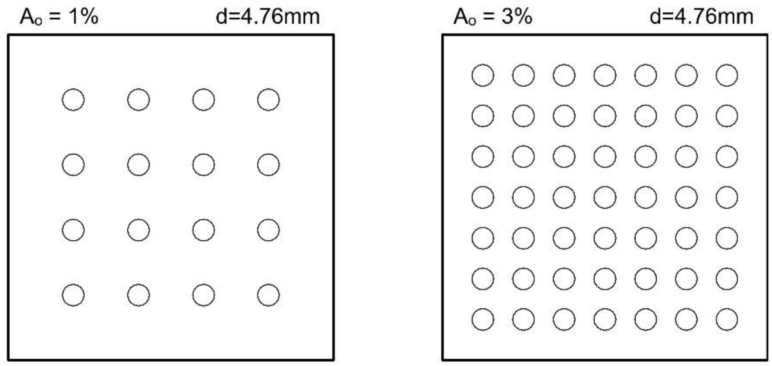

Figure 3: Jets arrays at $A_o = 1\%\ and\ 3\%$ and fixed diameters.

Alsaiari [1] measured the discharge coefficients for these plates. The values are reported in Table 1 below. The values of C_d were observed to be independent of Re_d.

d(mm)	n	C_D	Standard deviation	$d_e(mm)$
3.18	6	0.784	0.003	2.8
4.76	6	0.785	0.005	4.22
6.35	6	0.802	0.002	5.69

Table 1: Measured discharge coefficients.

An electric resistance heater was used to heat the test surface while the air jets cooled the test surface. The average heat transfer coefficient was calculated from steady-state power measurements. An aluminum grooved plate was used with dimensions of 152.4mm by 152.4mm and thickness of 12.7 mm. The grooved surface is the area between the triangular ribs. There are 21 grooved channels in the plate and the angle between the ribs is 90^o as shown in Fig. 4.

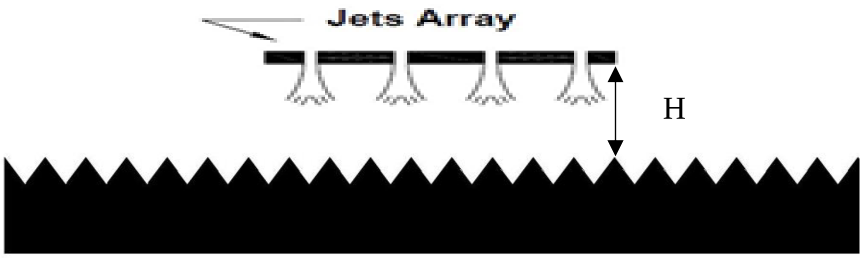

Figure 4: Test plate.

To ensure that the plate is heated uniformly, a total of 14 T-type thermocouples were made by welding the thermocouple wires and inserting them into small aluminum tubes with solder. They were then press fit into the test plate in different locations as shown in figure 5. Most of the thermocouples were mounted at the bottom of the grooves and a few in the top of the ribs and one into the side to ensure uniformity of temperature measurement.

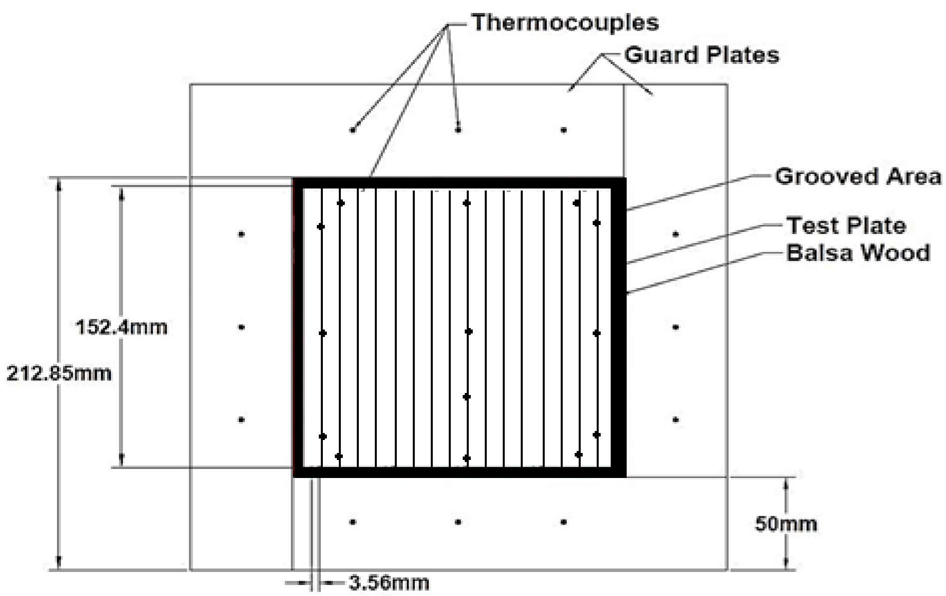

Figure 5: Top view of test Plate with guard plate and thermocouples locations.

Eight of the thermocouples were wired in parallel and supplied to Eurotherm 810 PID temperature controllers to control Eurotherm 831 Silicon Control Rectifiers (SCR), which in turn supplied power to the heaters. To measure the voltage E, it is important to use an RMS voltmeter (HP3486A) to determine the power supplied to the heater. After the voltage had been measured, the power was calculated as:

$$\text{Power} = \frac{E^2}{R} \tag{4}$$

Where R is the electrical resistance of the heater. The electrical resistance was constant with temperature over the operating range. By using an NI-9214 DAQ system, temperature readings from the remaining six thermocouples were recorded individually. By using additional PID controllers and SCR's, the four guard plates surrounding the test plate were maintained at the same set-point temperature as the test plate to minimize the edge losses. To minimize the conduction losses from the bottom of the plate, it was placed on a multilayer of insulation materials of wood and fiberglass. The system took about 15 minutes to reach steady state in the case of the dry experiments while it took about 25 minutes in the wet cases.

Data Analysis:

Heat transfer was calculated through steady-state experiments. Convection, radiation and evaporation heat transfer were calculated in the experiments. The surface temperature is constant at T_s= 42.8 ^{o} C. T_o is the air temperature of the jet array that hits the grooved plate. The grooves have the shape of triangles and may contain water. As shown in Fig. 6 the energy balance for the heat transfer is:

$$\text{Power} = q_{rad} + q_{evap} + q_{conv} + q_{losses} \tag{5}$$

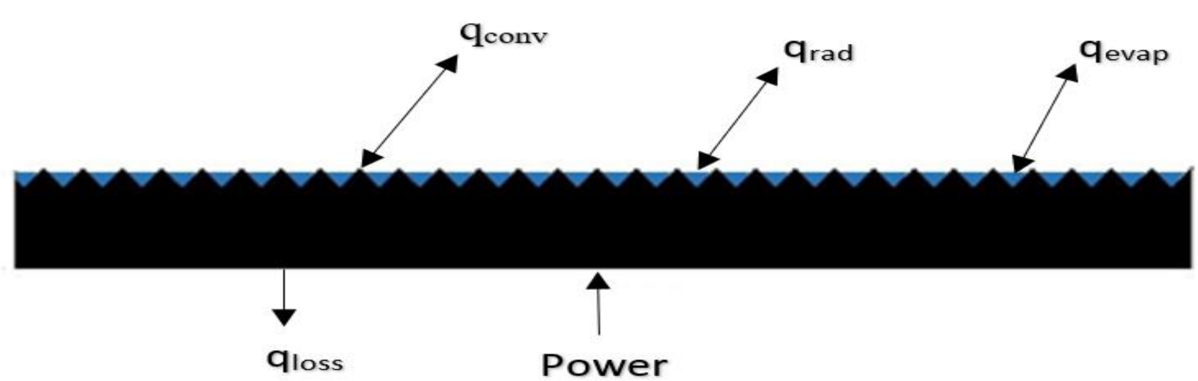

Figure 6: Energy balance and heat transfer mechanisms in hybrid jet impingement cooling

The radiation exchange for the dry surface is

$$q_{rad,dry} = \varepsilon_d \, \sigma \, A_d \, (T_s^4 - T_a^4) \tag{6}$$

where A_d = dry surface area and ε_d = the emissivity coefficient for the dry surface area which equals to 0.76 [1] and σ = 5.6703 10^{-8} (W/m^2K^4) - the Stefan-Boltzmann Constant. For the wet case the radiation is

$$q_{rad,wet} = \varepsilon_w \, \sigma \, A_w \, (T_s^4 - T_a^4) \tag{7}$$

where T= temperature in Kelvin and A_w is the wet surface area,

ε_w is the emissivity coefficient for the wet surface area and $\varepsilon_w = 0.96$. The areas are shown in Fig. 7.

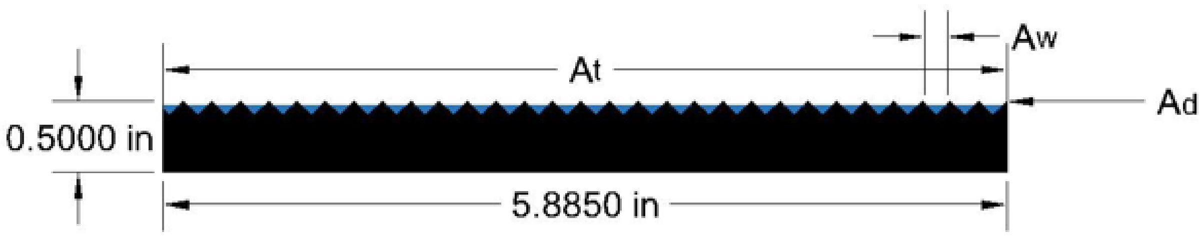

Figure 7: Plate dimensions.

The convection for the wet surface is $q_{conv,w} = h \, A_w(T_s - T_a)$ (8)

where h is the heat transfer coefficient. For the dry surface the convection is

$$q_{conv,d} = h \, A_d \, (T_s - T_a) \tag{9}$$

and the heat transfer by evaporation is

$$q_{evap} = h_m \, A_w \, i_{fg} \, (C_w - C_a) \tag{10}$$

Where $i_{fg}$is the latent heat of vaporization of water (2256 kJ/kg). h_m= mass transfer coefficient, C_s= concentration of the water in the air at the surface and C_a= concentration of the water in the air at the jet opening. Ø is the relative humidity. v_g is the specific volume for water vapor.

$$C_s = \left(\frac{1}{v_g}\right) \text{at } T_s \;\; and \;\; C_a = \left(\frac{\emptyset}{v_g}\right) \text{at } T_a. \tag{11}$$

From equation 5,

$$q_{evap} + q_{conv} = (Power - q_{rad} - q_{losses}) \tag{12}$$

This combination is defined as the total transfer to the air

$$q_{air} = q_{evap} + q_{conv} = (\mathrm{Power} - q_{rad} - q_{losses}) \tag{13}$$

The overall radiation from the wet and dry surfaces is

$$q_{rad} = \sigma\{\varepsilon_d A_d (T_s^4 - T_a^4) + \varepsilon_w A_w (T_s^4 - T_a^4)\} \tag{14}$$

$$q_{air} = h A_t (T_s - T_a) + h_m A_w i_{fg} (C_w - C_o) \tag{15}$$

where A_t is the summation of A_d and A_w, and A_t= A

The mass transfer coefficient is related to the heat transfer coefficient by the Lewis relation

$$h_m = h \left[\frac{D_{AB}\, Le^{1/3}}{K}\right] \tag{16}$$

where D_{AB}= mass diffusivity coefficient of water vapor in air

k= thermal conductivity ($W.m^{-1}.K^{-1}$) and Le= Lewis number = $\frac{\alpha}{D} = 0.865$.

From which the convection heat transfer coefficient is calculated as:

$$h = \frac{q_{air}/A}{(T_s - T_a) + \left(\frac{D_{AB}\, Le^{1/3}}{K}\right) \frac{Aw}{At} i_{fg} (C_s - C_a)} \tag{17}$$

The fan power is defined as

$$P_f = \frac{\forall\, \Delta P}{\eta\, f} \tag{18}$$

where $\forall$ is the air volume flow rate and η_f is the fan efficiency. η_f = 0.65

$$\forall = A_o\, A\;\; V \tag{19}$$

The coefficient of performance is defined as:

$$C_p = \frac{q_{air}}{P_f} \tag{20}$$

The Nusselt number was calculated as:

$$Nu = \frac{h\, d_e}{K}. \tag{21}$$

The average convection heat transfer coefficient for dry surface was calculated as:

$$h = \frac{q_{air}}{(T_s - T_a)\, A_s} \tag{22}$$

Where A_s is the test plate projected surface area of 152.4mm by 152.4mm as shown in figure 5.

The Reynolds number was calculated as:

$$Re = \frac{V.d_e}{\nu}. \tag{23}$$

Data Uncertainty:

Table 2 represents the sources of uncertainty in the measurement of Nu with the respective uncertainty values. Parameters were selected based on the expression that was adopted to calculate Nu such as:

$$Nu = \frac{h\, d_e}{k} = \frac{V^2/R}{\left[(\mathrm{T_s}-\mathrm{T_a})+\left(\frac{\mathrm{D_{AB}}\,\mathrm{Le}^{1/3}}{\mathrm{K}}\right)\frac{A_w}{A_t}\,\mathrm{i_{fg}}\,(\mathrm{C_s}-\mathrm{C_a})\right]}\,\frac{d_e}{k\,A_t} \qquad (24)$$

Therefore, the uncertainty on Nu was estimated as:

$$U_{n(NU)} = \left\{\left[\frac{\partial}{\partial V}(Nu).U_{nV}\right]^2 + \left[\frac{\partial}{\partial R}(Nu).U_{nR}\right]^2 + \left[\frac{\partial}{\partial d_e}(Nu).U_{nd_e}\right]^2 + \left[\frac{\partial}{\partial T}(Nu).U_{nT}\right]^2 + \left[\frac{\partial}{\partial A_t}(Nu).U_{nA_t}\right]^2 + \left[\frac{\partial}{\partial A_w}(Nu).U_{nA_w}\right]^2 + \left[\frac{\partial}{\partial K}(Nu).U_{nK}\right]^2 + \left[\frac{\partial}{\partial (\mathrm{D_{AB}})}(Nu).U_{n(\mathrm{D_{AB}})}\right]^2 + \left[\frac{\partial}{\partial \mathrm{Le}}(Nu).U_{n\mathrm{Le}}\right]^2 + \left[\frac{\partial}{\partial \mathrm{i_{fg}}}(Nu).U_{n\mathrm{i_{fg}}}\right]^2 + \left[\frac{\partial}{\partial \mathrm{C_s}}(Nu).U_{n\mathrm{C_s}}\right]^2 + \left[\frac{\partial}{\partial \mathrm{C_a}}(Nu).U_{n\mathrm{C_a}}\right]^2\right\}^{\frac{1}{2}} \qquad (25)$$

The resulting value of uncertainty was found to be 7% to 10% depending on the size of the Nu. Smaller Nu leads to larger uncertainty.

Source of uncertainty	Value	Unit
1. Voltage measurement, U_{nV}	0.02% of measured V	Volt
2. Resistance measurement, U_{nR}	0.5% of measured R	ohm
3. Orifice diameter measurement, U_{nd_e}	$4\text{x}10^{-5}$	m
4. Temperature measurement, U_{nT}	2.5	k
5. Surface area measurement, $U_{nA_{t,w}}$	$3.4\text{x}10^{-4}$	m^2
6. Thermal conductivity value, U_{nK}	$1.3\text{x}10^{-4}$	w/(m-k)
7. Mass diffusivity uncertainty, $U_{n(\mathrm{D_{AB}})}$	$0.04\text{x}10^{-5}$	m^2/s
8. Lewis number uncertainty, $U_{n\mathrm{Le}}$	0.04	–
9. Water latent heat uncertainty, $U_{n\mathrm{i_{fg}}}$	5.6	kj/kg
10. Water concentration at the surface, $U_{n\mathrm{C_s}}$	$7.33\text{x}10^{-7}$	kg/m^3
11. Water concentration in jet air, $U_{n\mathrm{C_a}}$	$5.06\text{x}10^{-7}$	kg/m^3

Table 2: Uncertainty sources for the wet surface

Results and Discussion:

Jet impingement experiments were conducted at constant surface temperature Ts=42.8 ^{o}C under dry/wet conditions. The average convection heat transfer coefficients were obtained using equation 17 for the wet case. For the dry case, the average heat transfer coefficient was calculated by using equation 22. The measured convection coefficients of the triangular grooved plate are compared to the convection coefficient measured at the rectangular grooved surface in [1] under the dry case. The goal is to characterize the resulting heat transfer under different conditions such as flow open area percentage, array orifices diameter and array to surface stand-off distance.

Results for dry grooved surface:

Jet velocities of 5m/s, 7.5m/s, 10m/s, and 20m/s were used with two stand-offs distance ratios H/de of 12.7 and 17. Table 3 shows the corresponding Reynolds number based on effective jet diameter was calculated using equation 22.

Velocity (V m/s)	Reynolds number R_e Effective diameters (d_e mm)		
	d_e =2.8mm	d_e = 4.22mm	d_e = 5.69mm
V= 5	9234	13918	18766
V=7.5	13852	20877	28149
V=10	18469	27837	37534

Table 3: Reynolds number.

Figures 8 and 9 show the variation of average heat transfer coefficient with velocities for the grooved surface at different H/d_e ratios and constant diameter d, open Area A_o and temperature T_s.

In figure 8, representative results compare the average heat transfer coefficient from two different plates of rectangular and triangular grooved surfaces. The rectangular grooved plate showed higher results in the average heat transfer than triangular plate at all different velocities. Higher jet velocity leads to higher heat transfer coefficient as expected.

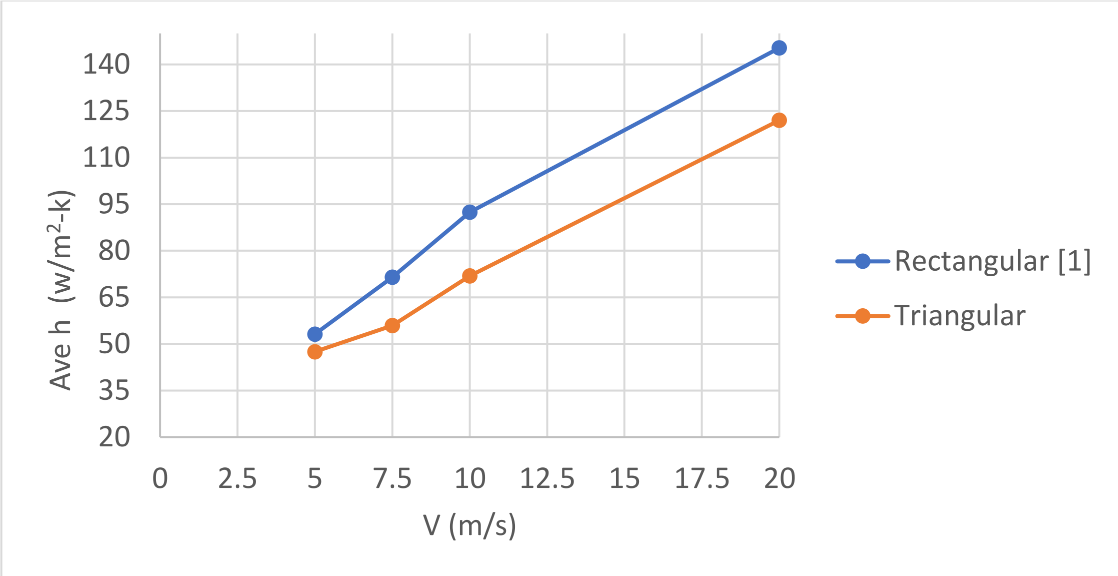

Figure 8: Average heat transfer coefficient vs Velocity

for H/d_e = 12.7, d_e =4.22mm, A_o= 1.5%.

In figure 9, H/d_e has been changed to 17 and all other conditions remain constant. Two different velocities were tested. The results show that the change of the H/d_e does not affect the fact that rectangular grooved plate has higher heat transfer than triangular plate under dry condition.

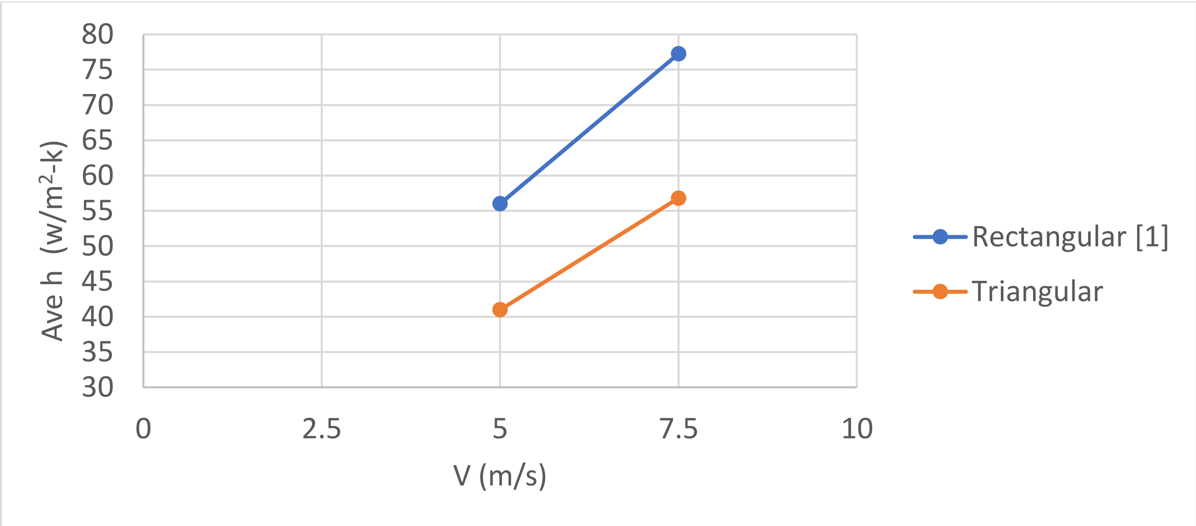

Figure 9: Average heat transfer coefficient vs Velocity

for H/d_e= 17, d_e=4.22 mm, A_o= 1.5%.

In figure 10, the diameter of the orifice plate has been decreased and experiments were conducted under same other conditions as figures 8 and 9. The larger H/d_e decreases the heat transfer coefficient, which is still lower than the rectangular grooved plate.

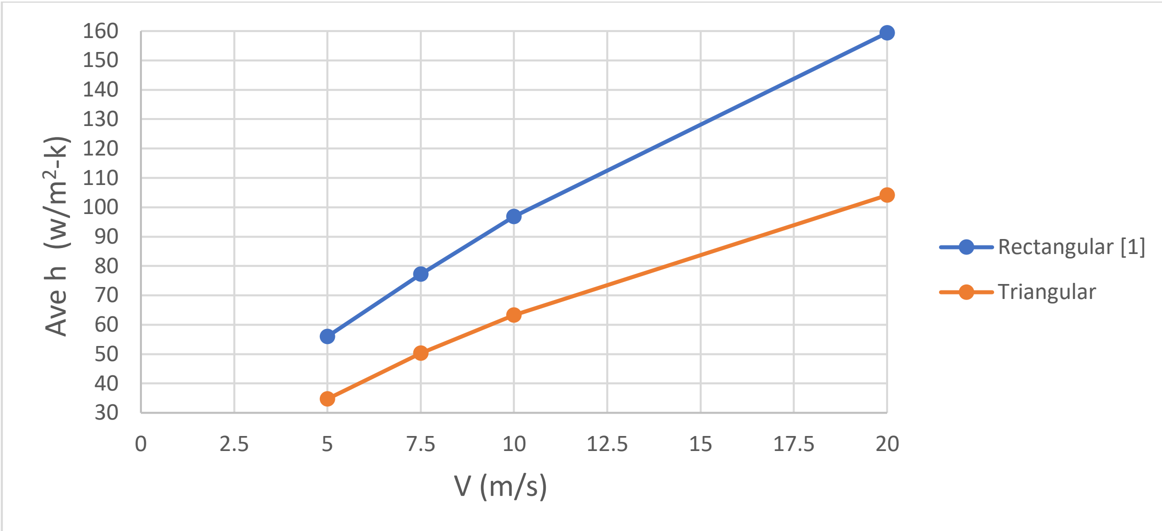

Figure 10: Average heat transfer coefficient vs Velocity

for H/d_e= 12.7, d_e=2.8 mm, A_o= 1.5%.

Figure 11 shows results with a larger diameter of the orifice plate under same conditions as shown in figure 10. The diameter has small improvement in heat transfer by using triangular grooved plate.

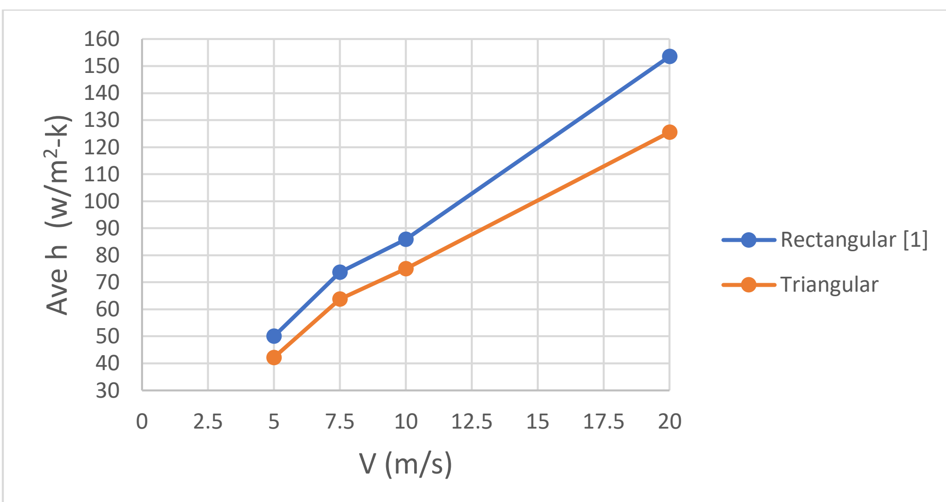

Figure 11: Average heat transfer coefficient vs Velocity

for H/d_e= 12.7, d_e=5.69 mm, A_o= 1.5%.

Another way of viewing the change of heat transfer is as a function of open area as shown in figure 12. Higher and lower open areas are compared on both rectangular and triangular surfaces. Figure 12 shows the result of rectangular and triangular plates at V= 5m/s at two different open areas.

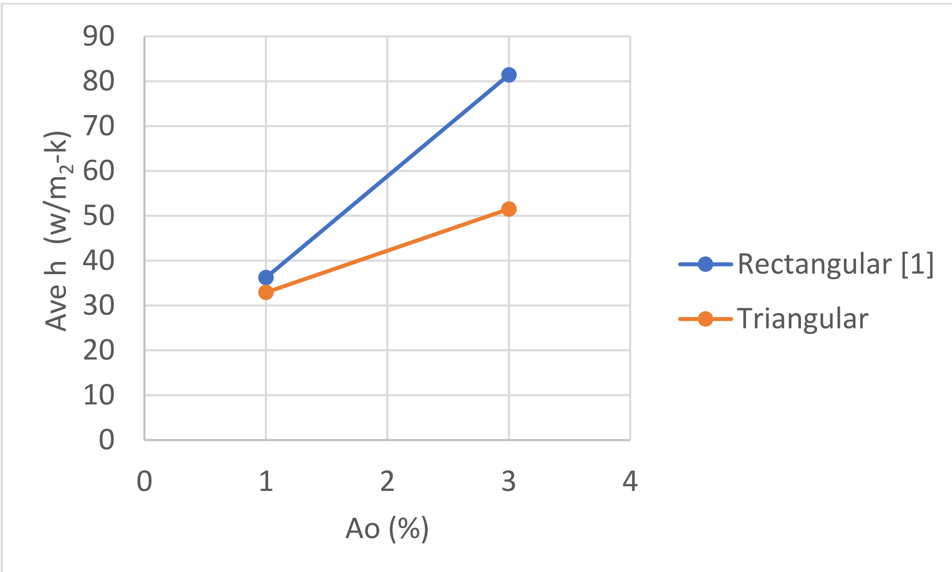

Figure 12: Average heat transfer coefficient vs Open area for H/d_e= 12.7, d_e=4.22 mm.

Results for triangular wet grooved surface:

Water was used to fill in the grooved channels to different depths, which gave different wet coverages. This is different than for the rectangular channels. As the ratio of wet area to the total area changes, the heat transfer coefficient and Nu changes. The q_{air} was used to show the change of the total energy transfer from the surface. Three different velocities were used in these experiments at V=5 m/s, 7.5m/s and 10m/s. Four different wet area ratios were used at A_w/A_t = 100%, 70%, 50% and 30%. Higher energy transfer was found to be in the ratio of 50% wet area. Highest average heat transfer coefficient and Nu were found in the ratio of 30%.

Figure 13 represents the total energy transfer at different wet ratios and velocities. As the velocity increases, the energy transfer increases. Figures 14, 15, 16, 17 and 18 have the same open area of A_o = 1.5% at different diameters and H/d_e. When the grooved channels are full of water A_w/A_t= 100%, the energy transfer has the lowest value. The energy transfer actually increases as the wet coverage decreases until it reaches the highest value at A_w/A_t= 50%. It decreases again when the ratio of A_w/A_t= 30% due to less evaporation. Heat flux was calculated by dividing q_{air} to total area of the test plate which is 0.0223 m^2. Highest heat flux was found at 50% wet coverage area at the highest velocity of 10 m/s.

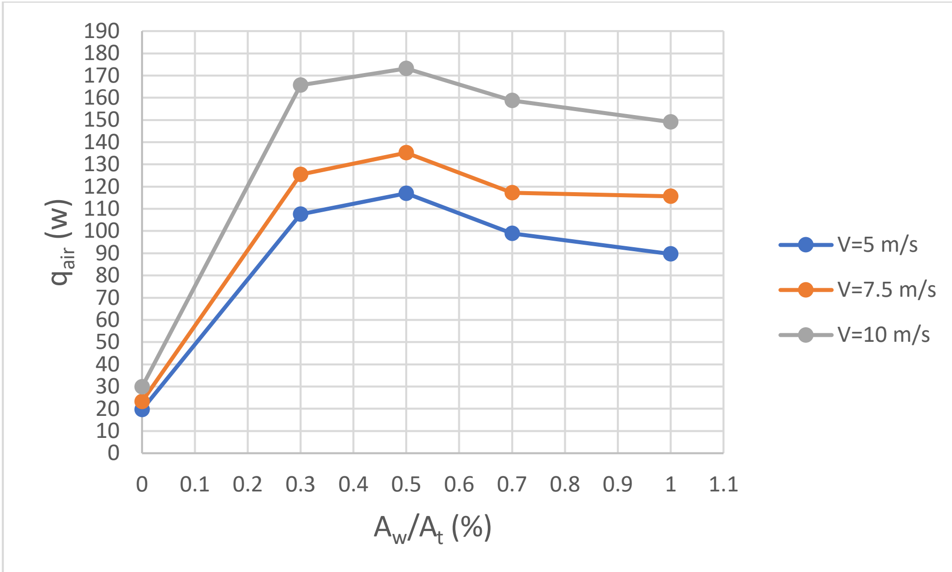

Figure 13: q_{air} vs A_w/A_t for H/d_e= 12.7, d_e=4.22 mm, A_o= 1.5%.

Figure 14 shows the average heat transfer coefficient under the same conditions of figure 13. The heat transfer coefficient increases as the ratio of wet area decreases. This explains why the maximum transfer occurs at 50% wet coverage.

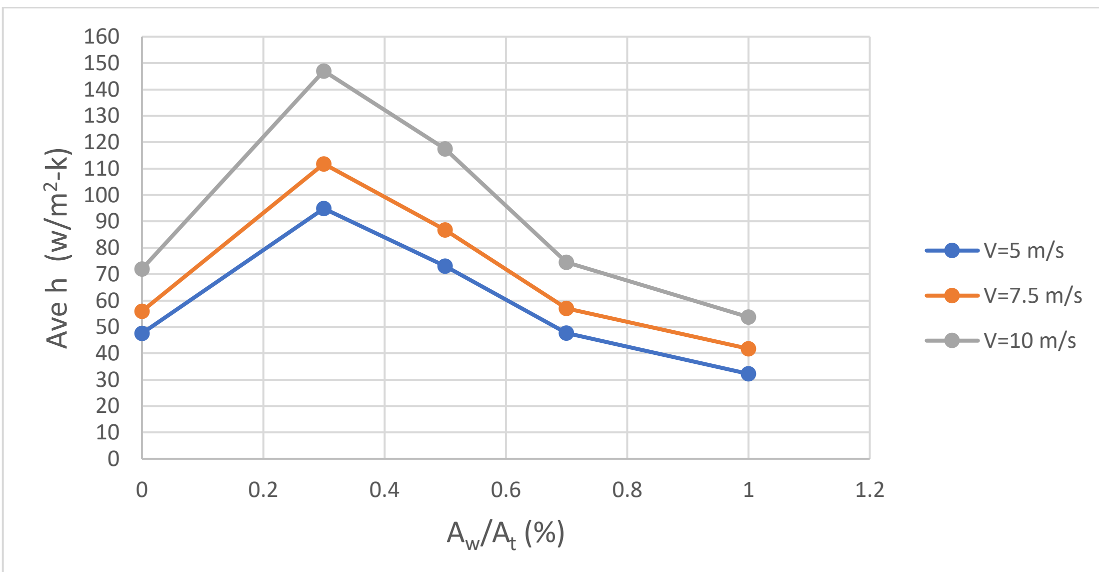

Figure 14: Heat transfer coefficient vs A_w/A_t for H/d_e= 12.7, de=4.22 mm, A_o= 1.5%.

H/d_e has been changed to test the enhancement of heat transfer at different array to surface stand-off distances. Figure 15 illustrates the variation of q_{air} at different conditions.

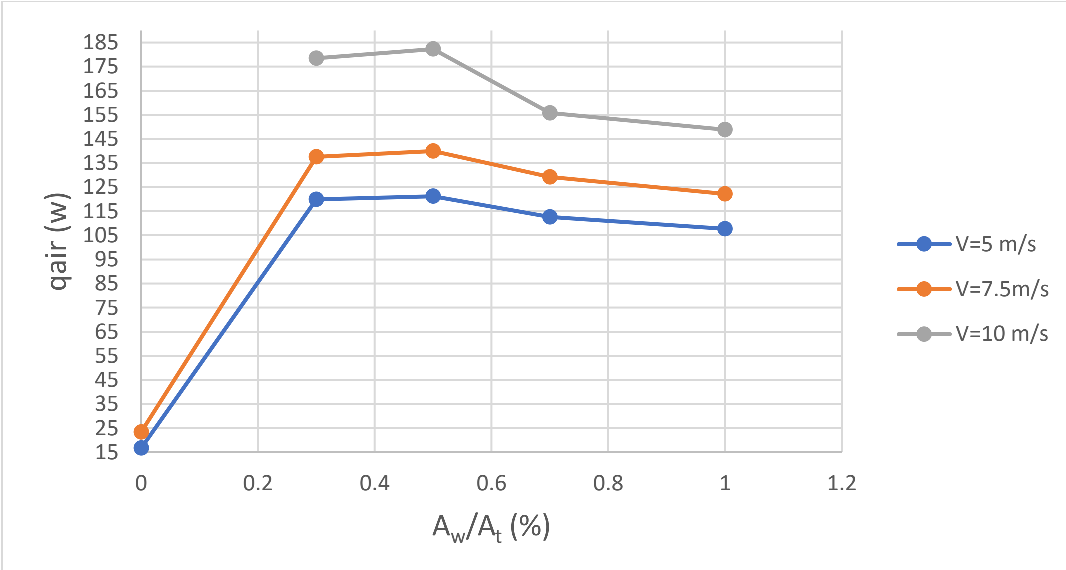

Figure 15: q_{air} vs A_w/A_t for H/d_e= 17, d_e=4.22 mm, A_o= 1.5%.

The variation of heat transfer coefficient was shown in figure 16 under the same conditions above. At H/d_e=17, higher heat transfer coefficient was found than H/d_e=12.7 at all different velocities.

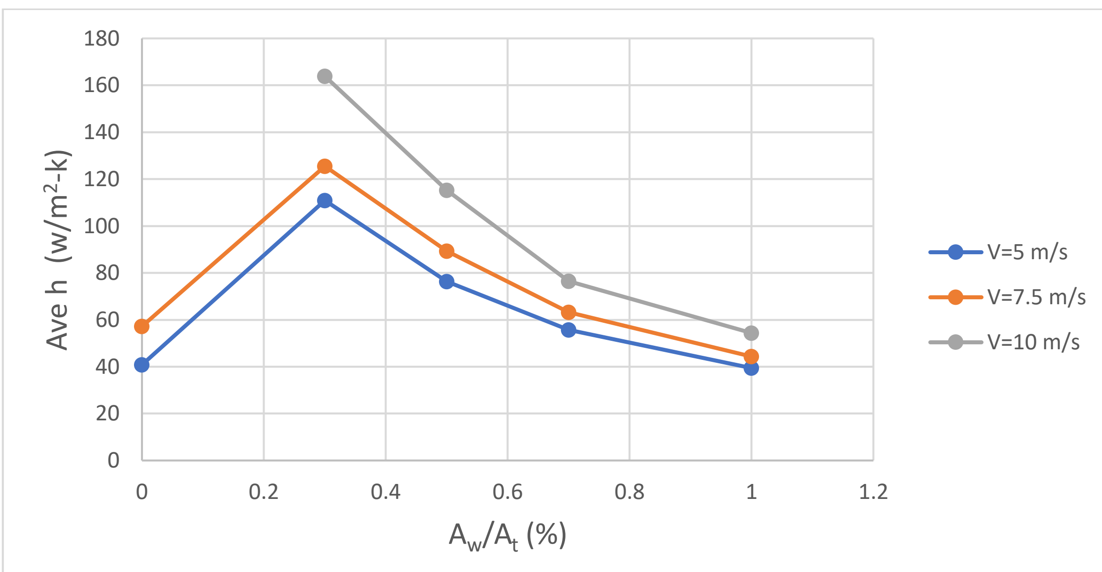

Figure 16: Heat transfer coefficient vs A_w/A_t for H/d_e= 17, de=4.22 mm.

An even larger H/d_e was used as shown in figure 17. We can see the variation between each point at all velocities, but that did not change the fact that highest level of energy transferwas found to be at the ratio A_w/A_t of 50%. We can conclude that the H/d_e has no effect on the wet coverage the gives the maximum value of q_{air} .

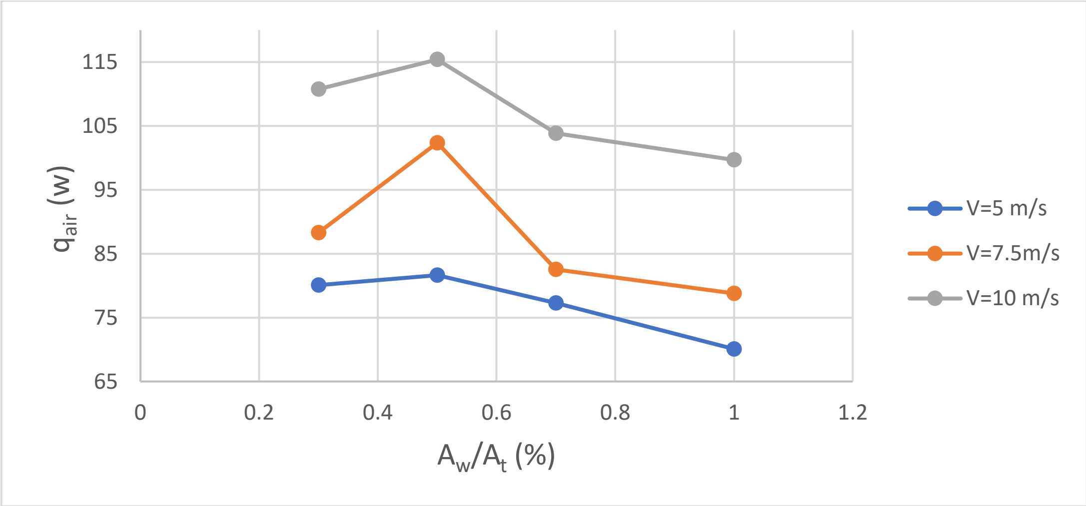

Figure 17: q_{air} vs A_w/A_t for H/d_e= 28.4, de=4.22 mm, A_o= 1.5%.

Figure 18 represents the heat transfer coefficient under the same experiment. As expected the H/d_e at 28.4 gave lower values ofheat transfer coefficient compared to H/d_e at 17.

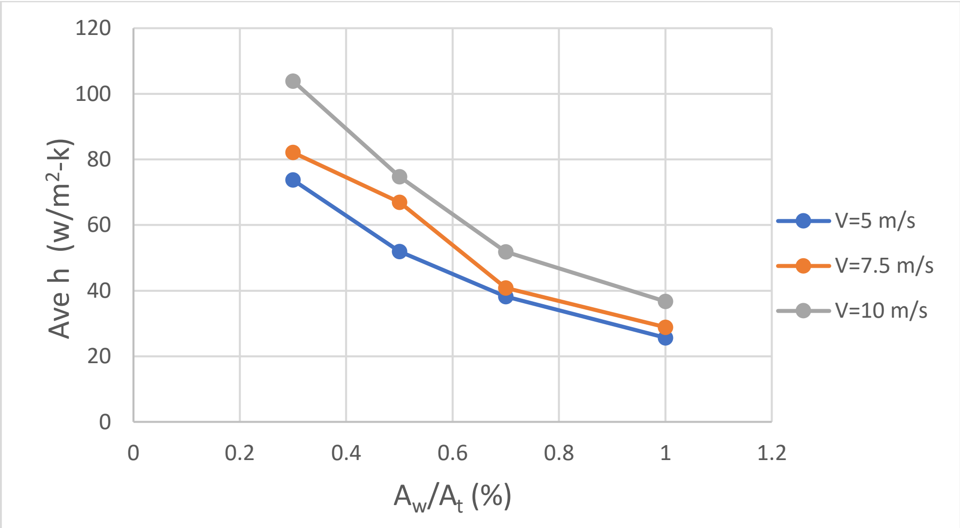

Figure 18: Heat transfer coefficient vs A_w/A_t for H/d_e= 28.4, d_e=4.22 mm, A_o= 1.5%.

Changing the orifice diameter tried to test the effect on the enhancement of heat transfer. Two new different orifice diameters of d_e=1/8 inch and 1/4 inch were tested.

Figure 19 represents the power vs the wet area ratios at different two velocities.

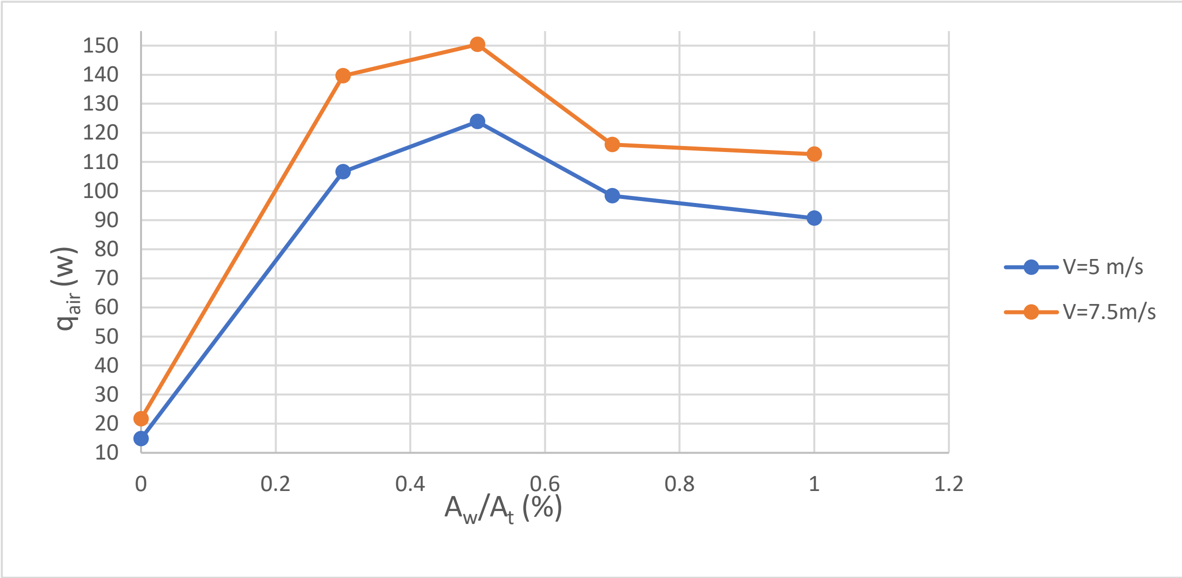

Figure 19: q_{air} vs A_w/A_t for H/d_e= 12.7, d_e=2.8 mm, A_o= 1.5%.

Under the same experiment, heat transfer coefficient is shown in figure 20 at two different velocities. Results show higher heat transfer coefficients at this different diameter plate.

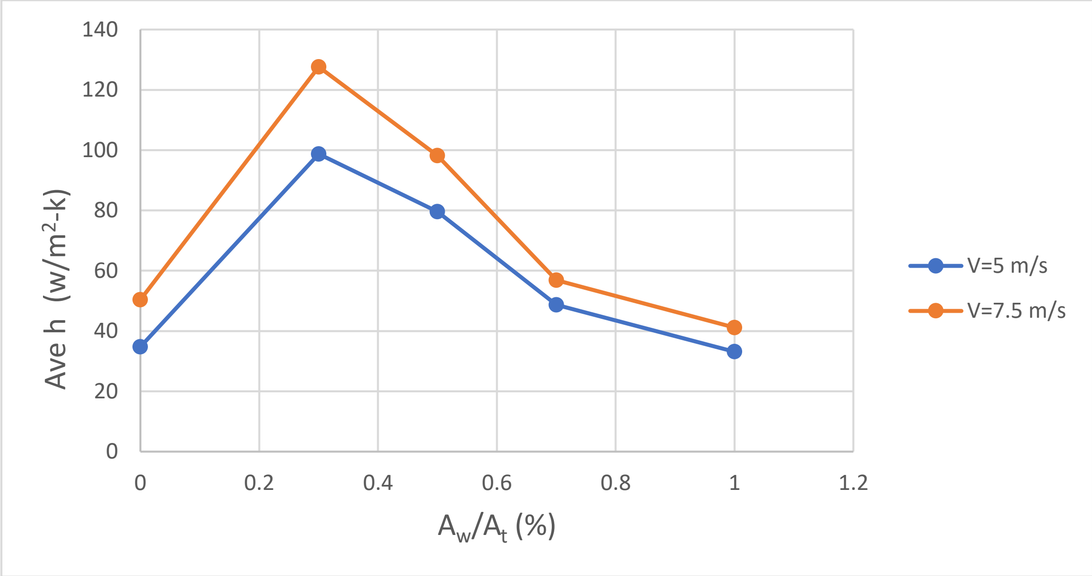

Figure 20: Heat transfer coefficient vs A_w/A_t for H/d_e= 12.7, d_e=2.8 mm, A_o= 1.5%.

The same experiments as shown in figure 17and 18 were conducted at an orifice diameter of d_e=1/4 inch as shown in figure 21. Both figures show that the change of the orifice diameters has no effect on the enhancement due to the change of the wet area ratios to the total area.

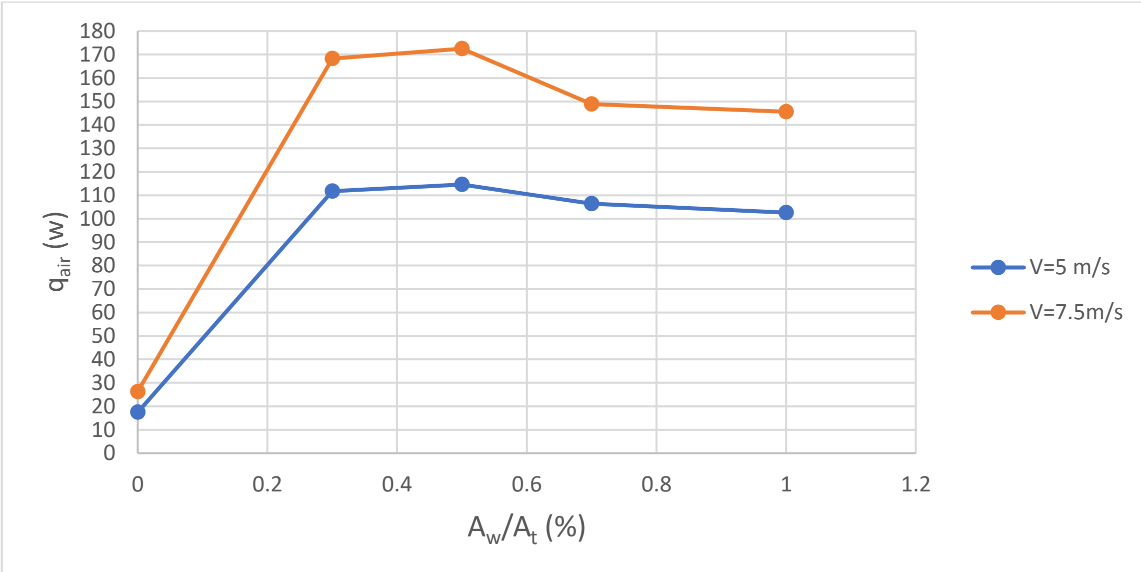

Figure 21: q_{air} vs A_w/A_t for H/d_e= 12.7, d_e=5.69 mm, A_o= 1.5%.

At different diameter, figure 22 shows higher heat transfer coefficient at d_e=5.69mm than other diameters.

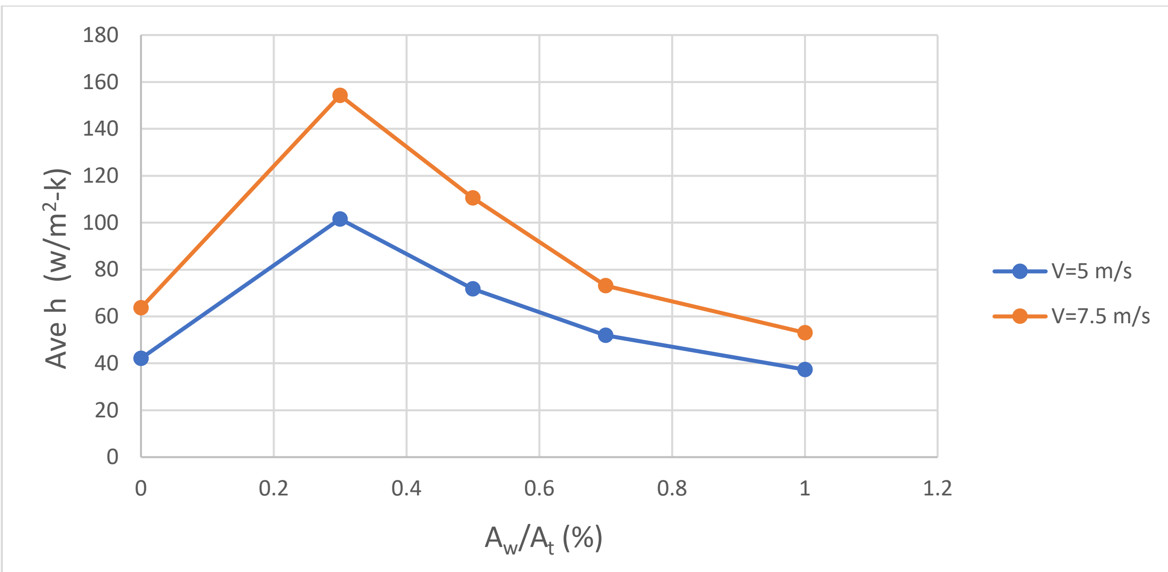

Figure 22: Heat transfer coefficient vs A_w/A_t for H/d_e= 12.7, d_e=5.69mm, A_o= 1.5%.

The last technique was used is to change the open area of the orifice plates. Open area of 1% and 3% were used. Figures 23,24,25 and 26 show the results respectively.

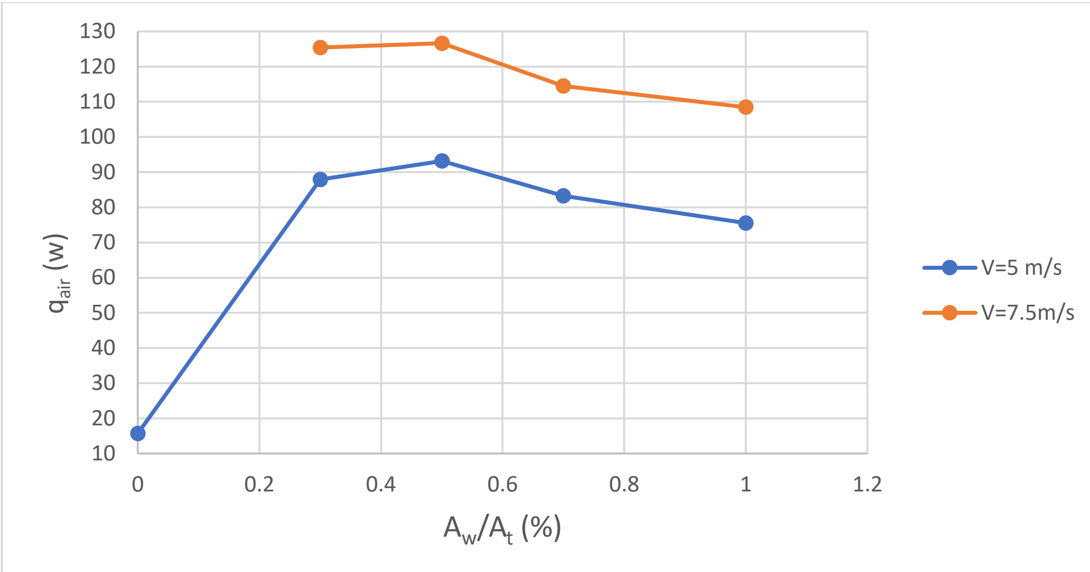

Figure 23: q_{air} vs A_w/A_t for H/d_e= 12.7, d_e=4.22 mm, A_o= 1%.

Figure 24 shows the new open area results. There is no improvement was noticed in heat transfer coefficient.

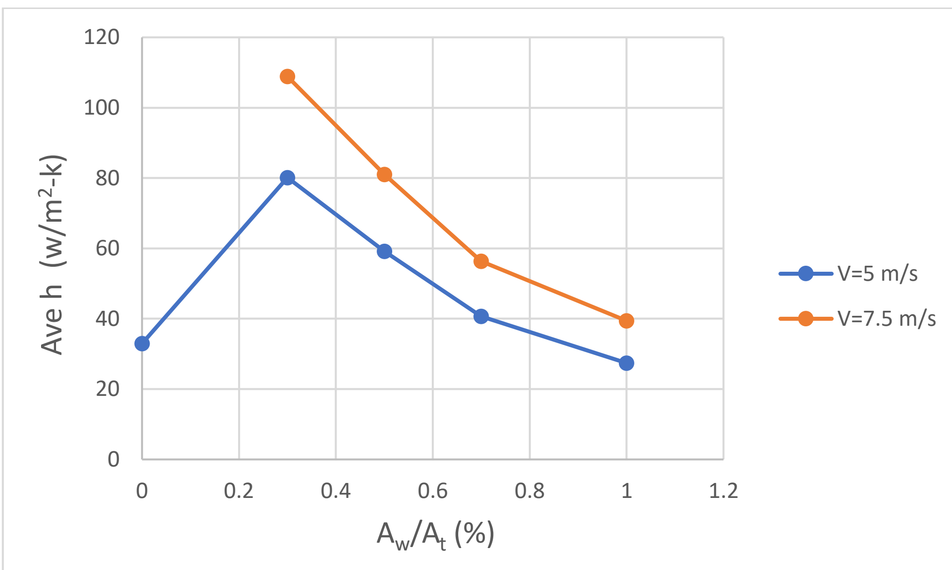

Figure 24: Heat transfer coefficient vs A_w/A_t for H/d_e= 12.7, d_e=4.22 mm, A_o= 1%.

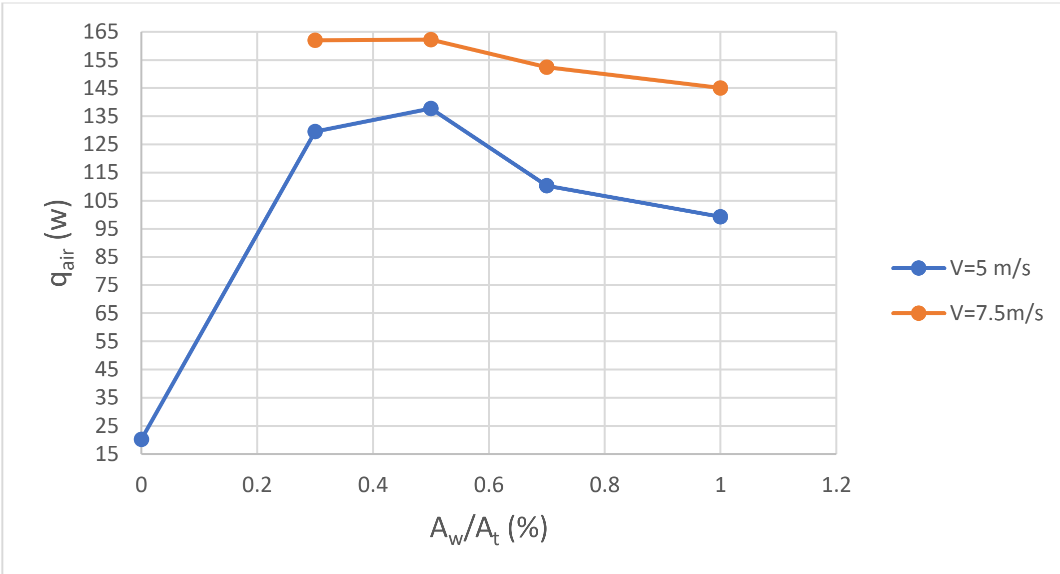

Figure 25: q_{air} vs A_w/A_t for H/d_e= 12.7, de=4.22 mm, A_o= 3%.

Figure 26 shows the heat transfer coefficient variation and it shows better results at open area= 3% than open area =1%.

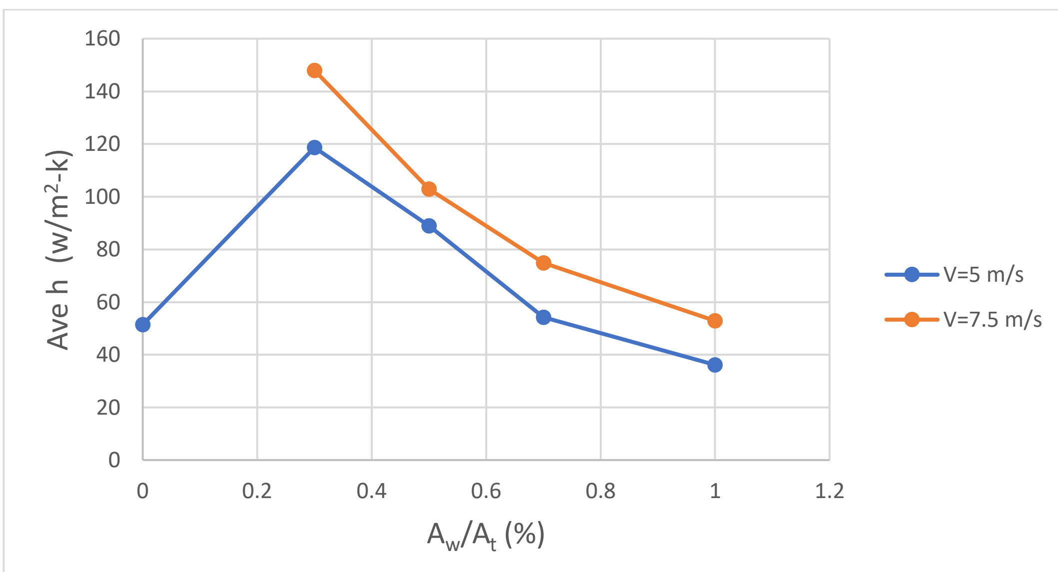

Figure 26: Heat transfer coefficient vs A_w/A_t for H/d_e= 12.7, d_e=4.22 mm, A_o= 3%.

The best results were found to be in the case of 50% wet grooved surface. Graphs below summarize the results under different conditions of A_o, d_e and H/d_e. Highest heat flux was found at 3% open area as shown in figure 27.

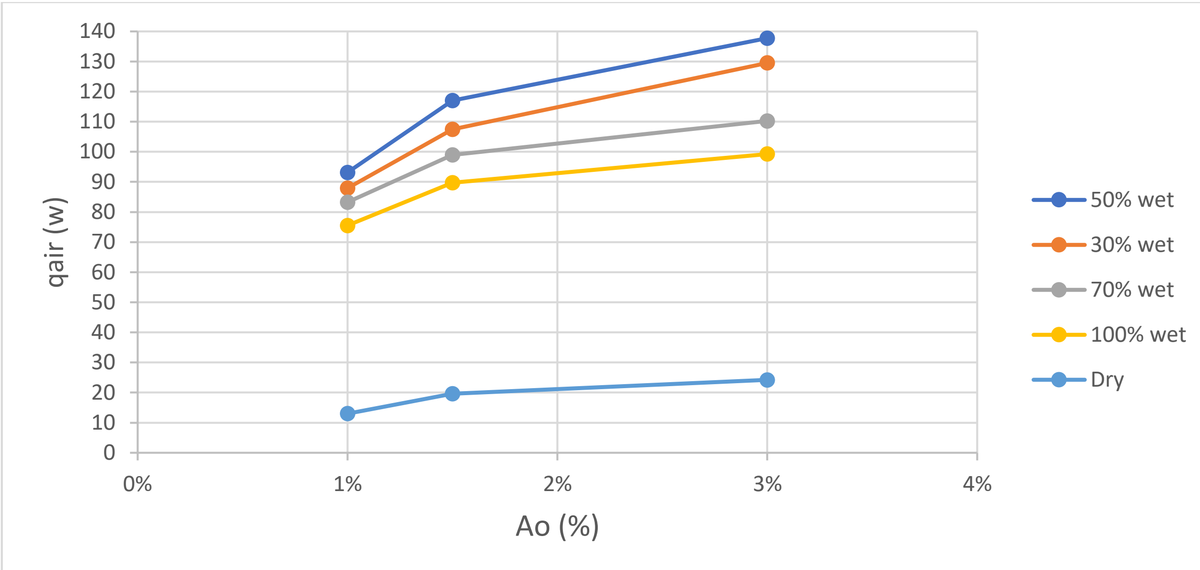

Figure 27: q_{air} vs Ao for V= 5 m/s, H/d_e= 12.7, de=4.22mm.

Figure 28 represents q_{air} under different d_e. Highest value was found to be in the effective diameter of 1/8 inch.

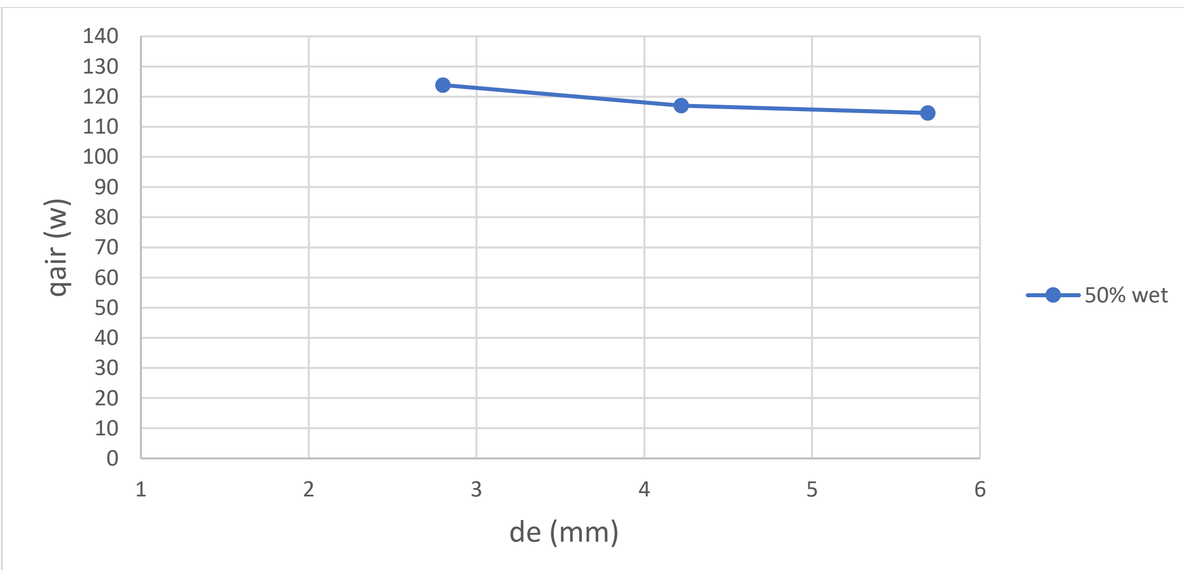

Figure 28: q_{air} vs d_e for V= 5 m/s, H/d_e= 12.7, A_o= 1.5%.

Figure 29 shows the q_{air} under different H/d_e. Highest q_{air} was found to be as shown in figure below at 17.

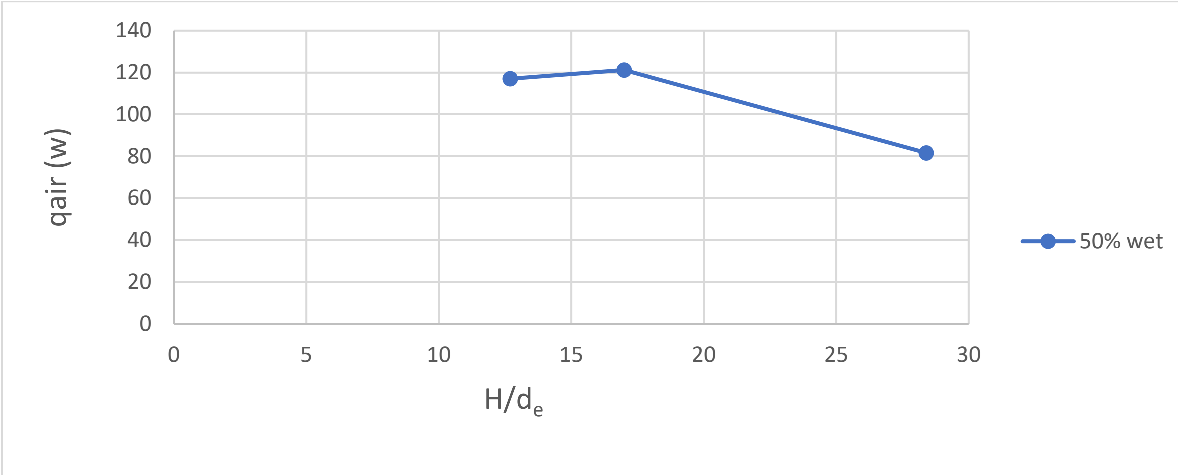

Figure 29: q_{air} vs H/d_e for V= 5 m/s, de=4.22 mm, A_o= 1.5%.

CP values were calculated and best results were found to be at 50% wet coverage areas.

Table 4 lists the CP values under different conditions. CP values showed 40% to 50% improvement as compared to [1].

CP values	100% wet coverage	70% wet coverage	50% wet coverage	30% wet coverage	Dry
V=5 m/s, H/d_e=12.7, d_e=4.22 mm	3210	3538	4184	3846	561
V=7.5 m/s, H/d_e=12.7, d_e=4.22 mm	1091	1116	1318	1188	160
V=5 m/s, H/d_e=17, d_e=4.22 mm	2998	3136	3374	3338	396
V=5 m/s, H/d_e=12.7, d_e=2.8 mm	2583	2803	3529	3038	411

Table 4: CP values under dry and wet conditions

Conclusions:

A new approach to cooling with hybrid jet impingement has been suggested and developed as an option for thermoelectric power plant steam condensers. The jets cooled a grooved surface with the grooves containing water at a constant temperature. The analogy for mass transfer offered detailed predictions for the simultaneous heat and mass transfer process. Large magnitudes of heat flux were observed using hybrid jet impingement cooling at low jet speeds and flow rates. The highest values of heat transfer coefficient were found at a wet coverage of A_w/A_t =30%. The highest total energy transfer was at a wet coverage of A_w/A_t = 50%. CP values from the wet case showed 100% improvement as compared to CP values for rectangular channels in [1]. CP > 4000 was observed in this study. The proposed approach allows water to be used efficiently since the energy of evaporation is absorbed from the steam and is not used to cool air as in conventional evaporative cooling. The cooling of the hybrid jet impingement is not restricted by the temperature of the wet bulb as is the case with the cooling towers, the spray cooling and the mist cooling. The results encourage the use of hybrid jet impingement in thermoelectric power plant condensers and other related fields, such as air conditioning and refrigeration. Some disadvantages of the system still need to be addressed; such as fouling of the surfaces over time.

Nomenclatures:

A= area (m^2)

A_t= total area (m^2)

A_w= wet area (m^2)

R= resistance (ohm)

E= voltage (volts)

σ = 5.6703 10^{-8} (W/m^2K^4) - The Stefan-Boltzmann Constant

T= temperature (k)

i_{fg}= latent heat of vaporization of water is (J/kg)

h_m= mass transfer coefficient (m^2/s)

C= concentration of the water (kg/m^3)

h= heat transfer coefficient ($w/m^2 k$)

D_{AB}= mass diffusivity coefficient (m^2/s)

K= thermal conductivity ($W.m^{-1}.K^{-1}$)

$\alpha =$ thermal diffusion (m^2/s)

$P_f =$ fan power (w)

q= heat transfer (w)

$q_{air} =$ total heat transfer (w)

∀= air volume flow rate (m^3/s)

V= velocity (m/s)

$A_s =$ test plate projected surface area (mm)

ν = kinematic viscosity of air (m^2/s)

Non-dimensional:

A_o= open area percentage (%)

Cp= coefficient of performance

$C_d =$ discharge coefficient = 0.000026

ε = emissivity coefficient

Le= Lewis number

N= number of jets

$N_{u=}$nusselt number

η f = fan efficiency

R_e= Reynolds number

Subscripts:

Cond = conduction

Conv = convection

Evap = evaporation

Rad = radiation

References:

[1] Alsaiari, A. O. (2018). Augmentation of Jet Impingement Heat Transfer on a Grooved Surface Under Wet and Dry Conditions. 91.

[2] J. Rogers, K. Averyt, S. Clemmer, M. Davis, F. Flores-Lopez, P. Frumhoff, D. Kenney, J. Macknick, N. Madden, J. Meldrum, Water-smart power: Strengthening the US electricity system in a warming world, Camb. MA Union Concerned Sci. (2013).

[3] Martin, H. (1977). Heat and mass transfer between impinging gas jets and solid surfaces. In Advances in heat transfer (Vol. 13, pp. 1-60). Elsevier.

[4] Gardon, R., & Akfirat, J. C. (1966). Heat transfer characteristics of impinging two-dimensional air jets. Journal of Heat Transfer, 88(1), 101-107.

[5] Goldstein, R. J., & Timmers, J. F. (1982). Visualization of heat transfer from arrays of impinging jets. International Journal of Heat and Mass Transfer, 25(12), 1857-1868.

[6] Hrycak, P. (1983). Heat transfer from round impinging jets to a flat plate. International Journal of Heat and Mass Transfer, 26(12), 1857-1865.

[7] Korger, M., & Křížek, F. (1966). Mass-transfer coefficient in impingement flow from slotted nozzles. International Journal of Heat and Mass Transfer, 9(4), 337-344.

[8] Snedeker, R. S. (1971). A study of free jet impingement. Part 1. Mean properties of free and impinging jets. Journal of fluid Mechanics, 45(2), 281-319.

[9] Hrycak, P. (1981). Heat transfer from a row of impinging jets to concave cylindrical surfaces. International Journal of Heat and Mass Transfer, 24(3), 407-419.

[10] Gau, C., & Chung, C. M. (1991). Surface curvature effect on slot-air-jet impingement cooling flow and heat transfer process.

[11] Gau, C., & Lee, C. C. (1992). Impingement cooling flow structure and heat transfer along rib-roughened walls. International Journal of Heat and Mass Transfer, 35(11), 3009-3020.

[12] N.P. Cheremisinoff, P.N. Cheremisinoff, Cooling towers selection, design and practice, Ann Arbor Science,Ann Arbor, MI, United States, 1981. https://www.osti.gov/servlets/purl/5913547.

[13] J.G. Bustamante, A.S. Rattner, S. Garimella, Achieving near-water-cooled power plant performance with air-cooled condensers, Appl. Therm. Eng. 105 (2016) 362–371. doi:10.1016/j.applthermaleng.2015.05.065.

[14] S. Taghian Dehaghani, H. Ahmadikia, Retrofit of a wet cooling tower in order to reduce water and fan power consumption using a wet/dry approach, Appl. Therm. Eng. 125 (2017) 1002–1014. doi:10.1016/j.applthermaleng.2017.07.069

[15] J. Maulbetsch, M. DiFilippo, Spray enhancement of air cooled condensers, EPRI Palo Alto CA Calif. Energy Commision Sacram. CA Crockett Cogener. (2003).

[16] J.A. Heyns, Performance characteristics of an air-cooled steam condenser incorporating a hybrid (dry/wet) dephlegmator, (2008).

Appendix:

Some comparation between two different plates for the dry case:

Starting with the orifice plate which has diameter of 3/16 inch and open area 1.5%.

1/ H/d_e= 5.4 cm, Ts= 42.8

Velocity	Rectangular Grooves	Triangular Grooves
V=5	Ave h=53.15 , ave Nu=8.5	Ave h=47.5 , ave Nu=7.6
V=7.5	Ave h=71.5 , ave Nu=11	Ave h=55.9 , ave Nu=8.5
V=10	Ave h=92.4 , ave Nu=14.8	Ave h=71.9 , ave Nu=11.5
V=20	Ave h=145.3 , ave Nu=23.2	Ave h=122 , ave Nu=19.5

H/d_e= 7.18

Velocity	Rectangular Grooves	Triangular Grooves
V=5	Ave h=45.25 , ave Nu=7.25	Ave h=40.97 , ave Nu=6.56
V=7.5	Ave h=76 , ave Nu=12.18	Ave h=56.8 , ave Nu=9.1

Second, the orifice plate which has diameter of 1/8 inch and open area 1.5%.

Velocity	Rectangular Grooves	Triangular Grooves
V=5	Ave h=56 , ave Nu=5.9	Ave h=34.72 , ave Nu=3.71
V=7.5	Ave h=77.24 , ave Nu=8.25	Ave h=50.3 , ave Nu=5.3
V=10	Ave h=96.8 , ave Nu=10.3	Ave h=63.2 , ave Nu=6.7
V=20	Ave h=159.4 , ave Nu=17	Ave h=104.1 , ave Nu=11.1

Third, the orifice plate which has diameter of 1/4 inch and open area 1.5%.

Velocity	Rectangular Grooves	Triangular Grooves
V=5	Ave h=50.39 , ave Nu=10.89	Ave h=42.17 , ave Nu=9.11
V=7.5	Ave h=73.68 , ave Nu=15.93	Ave h=63.72 , ave Nu=13.77
V=10	Ave h=85.92 ,ave Nu=18.57	Ave h=75.01 , ave Nu=66.21
V=20	Ave h=153.53 ,ave Nu=33.19	Ave h=125.5 , ave Nu=27.13

New experiment was conducted for different open area, 3% and diameter 3/16 inch.

H/d_e= 5.4 cm, Ts= 42.8.

Velocity	Rectangular Grooves	Triangular Grooves
V=5	Ave h=81.40 , ave Nu=13.05	Ave h=51.50 , ave Nu=8.25

New experiment was conducted for different open area, 1% and diameter 3/16 inch.

H/d_e= 5.4 cm, Ts= 42.8.

Velocity	Rectangular Grooves	Triangular Grooves
V=5	Ave h=36.2 , ave Nu=5.8	Ave h=32.9 , ave Nu=5.2

Wet case has been tested under different wet coverage areas.

Here is some comparison of all different levels of coverage and different conditions such as:

T_s= 42.8 °C for all tests. H/d_e =12.7, d=3/16 inch and A_o= 1.5%

Velocity	100% wet cov	70%	50%	30%
5 m/s	Ave h=32.2 Nu=5.1	Ave h =47 Nu=7.7	Ave h=72.9 Nu=11.77	Ave h=94.9 Nu=15.24
7 m/s	Ave h =41.7 Nu=6.7	Ave h =57 Nu=9.17	Ave h=86.8 Nu=13.94	Ave h=111.8Nu=17.9

H/d_e = 17, and the other conditions remain constant.

Velocity	100% wet cov	70%	50%	30%
5 m/s	Ave h=39.4 Nu=6.33	Ave h =55.7 Nu=8.9	Ave h=76.3 Nu=12.2	Aveh=110.9Nu=17.8
7 m/s	Ave h =44.3 Nu=7.1	Ave h=63.2 Nu=10.1	Ave h=89.2 Nu=14.3	Ave h=125.5Nu=20.1

d= 1/8 inch and the other conditions remain constant as the first test.

Velocity	100% wet cov	70%	50%	30%
5 m/s	Ave h=33.1 Nu=5.3	Ave h =48.7 Nu=7.8	Ave h=79.3 Nu=12.7	Aveh=98.9Nu=15.8
7 m/s	Ave h =41.3 Nu=6.6	Ave h=56.8 Nu=9.1	Ave h=89.2 Nu=15.7	Ave h=125.5Nu=20.5

A_o= 1 % and the other conditions remain constant as the first test.

Velocity	100% wet cov	70%	50%	30%
5 m/s	Ave h=27.3 Nu=4.4	Ave h =40.7 Nu=6.5	Ave h=59.1 Nu=9.4	Aveh=80.1Nu=12.8
7 m/s	Ave h =39.4 Nu=6.3	Ave h=56.3 Nu=9.	Ave h=81 Nu=9	Ave h=108.8Nu=17.5